PAPER

Check for updates

Polymorphism of Au₁₁(PR₃)₇Cl₃ clusters: understanding C−H···π interaction and C−H···Cl−C van der Waals interaction on cluster assembly by surface modification†

Chenwanli Qin,[ab] Qianqin Yuan,[ab] Peng Li, [ID] *[ab] Shuxin Wang, [ID] [ab] Shuang Chen *[abc] and Manzhou Zhu [ID] *[ab]

The C−H···π interaction and the C−H···Cl−C van der Waals interaction play a crucial role in the crystallization of nanoclusters. In this paper, we present an example of a crystal system transformation of Au₁₁(PR₃)₇Cl₃ from monoclinic (M) to trigonal (T) by surface modification. Atomically-resolved gold nanoclusters containing tris(4-chlorophenyl)phosphine and chloride ligands were synthesized and determined to be Au₁₁(*p*-ClPPh₃)₇Cl₃ (*p*-ClPPh₃ = tris(4-chlorophenyl)phosphine) by X-ray crystallography. Crystal data demonstrated that the C−H···Cl−C interaction is dominant in a trigonal crystal system of Au₁₁(*p*-ClPPh₃)₇Cl₃ with a R$\bar{3}$ space group. However, the C−H···π interaction is the major driving force to form a monoclinic crystal system of Au₁₁(PPh₃)₇Cl₃ (PPh₃ = triphenylphosphine) with a P2(1)/*n* space group. Moreover, UV-vis absorption spectra and X-ray photoelectron spectra reveal that the electronic structure of the Au₁₁(*p*-ClPPh₃)₇Cl₃ nanocluster is greatly influenced by *p*-ClPPh₃. This work provides critical implications for the crystallization of metal nanoclusters, as well as a better understanding of the non-covalent interaction on the nanocluster assembly and the crystal engineering by surface modification.

Introduction

Atomically precise noble metal nanoclusters have received widespread attention due to their peculiar applications, such as catalysis, energy conversion, and biomedicine.[1–6] Recently, experimental and theoretical studies of metal nanoclusters have witnessed tremendous progress. More importantly, the structure of these nanoclusters can be identified by single-crystal X-ray diffraction (SC-XRD).[7–10] Based on this advantage, it is possible to probe the structure details and the structure-related properties at the atomic level, which is highly desirable to further practical applications.[11–13]

Ligands play a crucial role in the stabilization of nanoclusters.[14–17] The non-covalent interactions between surface ligands not only alter properties of clusters but also have significant effects on nanocluster assembly and self-assembly.[18–30] For instance, Wu and co-workers demonstrated that C−H···π interactions facilitated the chiral arrangement of ligands, and the assembled ligands presented rotational and parallel patterns on the surface of the nanoparticles.[14] Pradeep and colleagues reported that C−H···π interactions are dominant in a cubic lattice and result in a higher luminescence efficiency.[16] Crudden *et al.* showed that multiple C−H···π and π···π interactions rigidify the ligands and contribute to the high photoluminescent quantum yields in the Au₁₃ nanocluster.[31] Zheng *et al.* reported that π···π interactions play a crucial role in stabilizing silver nanoclusters.[32] Xie *et al.* found that the assembly behaviour of clusters can be regulated by metal ions (*i.e.*, Ag⁺/Cs⁺).[33] Non-covalent interactions play an important role in nanocluster chemistry.[34,35] To date, a series of Au₁₁(PR₃)Cl₃ nanoclusters with adjustable ligands have been extensively studied comparing with other nanoclusters.[15,36–39] Therefore, Au₁₁(PR₃)Cl₃ clusters are chosen as models to investigate non-covalent interactions in the crystallization of nanoclusters by surface modification.

In the following, we synthesized Au₁₁(*p*-ClPPh₃)₇Cl₃ (**Au₁₁-Cl** for short) and Au₁₁(PPh₃)₇Cl₃ (**Au₁₁-H** for short) nanoclusters by using tris(4-chlorophenyl)phosphine and triphenylphosphine as the protecting ligand. The composition of the **Au₁₁-Cl** was

ᵃDepartment of Chemistry and Centre for Atomic Engineering of Advanced Materials, Anhui Province Key Laboratory of Chemistry for Inorganic/Organic Hybrid Functionalized Materials, Anhui University, Hefei, Anhui, 230601, P. R. China. E-mail: peng-li@ahu.edu.cn; chenshuang@ahu.edu.cn; zmz@ahu.edu.cn

ᵇKey Laboratory of Structure and Functional Regulation of Hybrid Materials, Anhui University, Ministry of Education, Hefei, 230601, P. R. China

ᶜInstitutes of Physical Science and Information Technology, Anhui University, Hefei, Anhui, 230601, P. R. China

† Electronic supplementary information (ESI) available. CCDC 1966633. For ESI and crystallographic data in CIF or other electronic format see DOI: 10.1039/d0ra01288b

characterized by electron spin ionization (ESI-MS), and the structure of the **Au₁₁-Cl** was determined by X-ray crystallography. We are engaged in illuminating the crystal system transformation ascribed to C–H⋯Cl–C interactions and C–H⋯π interactions. The different patterns of non-covalent interactions can alter the packing of nanoclusters into monoclinic or trigonal lattice. The distance between H and H atom (D_{HH} for short) reveals the non-covalent interactions of the intramolecular can also be changed through surface modification. Furthermore, UV-vis absorption spectra and X-ray photoelectron spectra reveal the difference in the electronic structure due to surface modification.

Experimental

Chemicals

All chemicals are commercial and were used without further purification. Hydrogen tetrachloroaurate tetrahydrate (HAuCl₄·4H₂O, 99.95%), triphenylphosphine (PPh₃, 98%), tris(4-chlorophenyl)phosphine (p-ClPPh₃, 98%), sodium borohydride (NaBH₄, 99.99%), methanol (HPLC grade, 99.9%) methylene chloride (HPLC grade, 99.9%), hexane (HPLC grade, 99.9%), ethanol (HPLC grade, 99.9%). Ultrapure water was purchased from Wahaha Co. Ltd. All glassware was cleaned with aqua regia (3 : 1 mix of hydrochloric acid and nitric acid), rinsed with ultrapure water, and then dried before use.

Synthesis of Au₁₁(p-ClPPh₃)₇Cl₃ (Au₁₁-Cl) and crystallization

First, HAuCl₄·4H₂O (157 mg, 0.4 mmol) was dissolved in 15 mL ethanol, tris(4-chlorophenyl)phosphine (0.15 g, 0.5 mmol) was dissolved in the solution. The solution was stirred (~1200 rpm) in a 50 mL round bottom flask. After stirring for 20 min, the solution colour turned turbid. Then, 5 mL ethanol solution of NaBH₄ (40 mg) was added, and the colour of solution changed from turbid to dark immediately. After stirring for 8 h, the organic solution was evaporated and washed several times with

hexane to remove the redundant phosphine and other by-products. Finally, The **Au₁₁-Cl** nanocluster was crystallized in vapour diffusion of hexane/CH₂Cl₂ at room temperature.

Synthesis of Au₁₁(PPh₃)₇Cl₃ (Au₁₁-H)

The Au₁₁(PPh₃)₇Cl₃ was synthesized according to the method in the literature by Hutchison *et al.*[36] First, AuCl(PPh₃) (500 mg) was dissolved in 15 mL ethanol solution and NaBH₄ (190 mg, 5 mmol dissolved) was slowly added to the solution. After stirring for 8 h, the organic solution was evaporated and washed several times with hexane to remove the excess PPh₃ and other by-products. The pure **Au₁₁-H** was red solid and crystallized in vapour diffusion of hexane/CH₂Cl₂ at room temperature.

Characterization

UV-vis spectra of nanoclusters in CH₂Cl₂ were performed on the UV-6000PC instrument.

Red-brown crystals were collected, and the structure of **Au₁₁-Cl** was determined by X-ray crystallography. Single crystal X-ray diffraction data of the **Au₁₁-Cl** was collected on a Bruker Smart 1000 CCD. The area detector used graphite-monochromatized Mo Kα radiation ($\lambda = 0.71069$ Å). A piece of red-brown block-shaped crystal (0.25 × 0.24 × 0.23 mm) was mounted onto a MiTeGen capillary with Fluorolube, and all structures were solved by direct methods using SHELXS-97. Data collection was performed under room temperature (296 K).

The electrospray ionization time-of-flight mass spectrometry (ESI-TOF-MS) measurement was recorded using UPLC H-Class XEVO G2 XS Qtof (Waters. Crop.). The **Au₁₁-Cl** was recorded in the positive ion mode when dissolving in CH₃OH, containing 50 mM CsOAc, and centrifugation for 5 min (12 000 rpm). The sample was infused at 180 μL h⁻¹. The source temperature was kept at 50 °C with the spray voltage keeping at 4 kV. The mass spectra were processed using Masslynx 4.1 software (Waters Corp.).
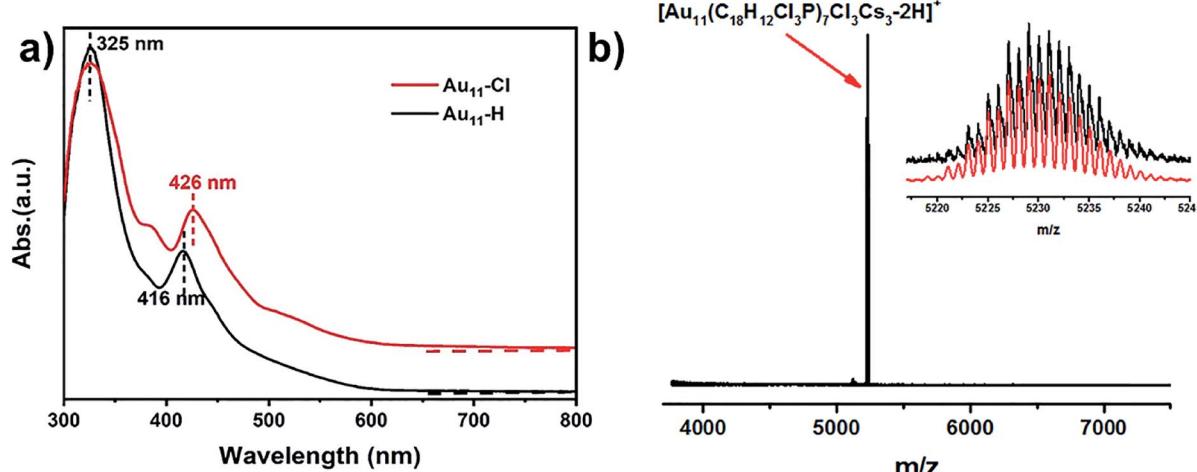

Fig. 1 (a) The UV-vis absorption spectra of **Au₁₁-Cl** and **Au₁₁-H**. (b) Positive ion mode ESI-TOF-MS of **Au₁₁-Cl** clusters in CH₃OH, inset: overlap of the experimental data (black) and the simulated spectrum (red) for **Au₁₁-Cl**.

The Thermo ESCALAB 250 instrument was used to measure X-ray photoelectron spectroscopy (XPS), which configured with a monochromated Al Kα (1486.8 eV) 150 W X-ray source, 0.5 mm circular spot size, and the analysis chamber base pressure lower than 1×10^{-9} mbar. Data were collected with FAT = 20 eV.

Results and discussions

As shown in Fig. 1a, the ultraviolet-visible (UV-vis) absorption spectrum of **Au$_{11}$-H** (black) shows two prominent peaks at 325 nm and 416 nm. While the UV-vis absorption spectrum of the **Au$_{11}$-Cl** (red) shows three peaks at 325 nm, 390 nm and 426 nm, respectively. The differences of absorption spectra possibly indicate that the electronic structure is distinctive, resulting from the replacement of PPh$_3$ by p-ClPPh$_3$. More, the thermodynamic stability of the Au$_{11}$ was explored under room temperature (Fig. S1†). These results imply the **Au$_{11}$-H** is more stable than **Au$_{11}$-Cl**. The formula of **Au$_{11}$-Cl** was confirmed by electrospray ionization time-of-flight mass spectrometry (ESI-TOF-MS). As shown in Fig. 1b, the ESI-TOF-MS (positive ion mode) revealed a single intense peak at m/z = 5230.02 Da, and the 1 gap between isotopic peaks proves that z = 1. The formula is attributed to $[\text{Au}_{11}(\text{C}_{18}\text{H}_{12}\text{Cl}_3\text{P})_7\text{Cl}_3\text{Cs}_3-2\text{H}]^+$ (**Au$_{11}$-Cl**). The experimental data matched well with the theoretical simulation indicates the purity of **Au$_{11}$-Cl**. X-ray photoelectron spectroscopy (XPS) was further performed to reveal the electronic structure of **Au$_{11}$-Cl** and **Au$_{11}$-H**. Fig. S2† shows the total spectra of XPS for

two nanoclusters. The Au 4f peak (84.53 eV) of **Au$_{11}$-Cl** nanocluster is on the higher energy side compared to that of **Au$_{11}$-H** (84.05 eV), which means the Au atoms in the **Au$_{11}$-Cl** are more oxidized than those in the **Au$_{11}$-H**.

The structure of **Au$_{11}$-Cl** was determined by the single crystal X-ray crystallography (Fig. 2). The molecular structure of the **Au$_{11}$-Cl** is similar to that of the **Au$_{11}$-H**. Ten gold atoms (yellow) form an incomplete icosahedral structure with one gold atom in the centre. And the ligands of six p-ClPPh$_3$ (pink) and three Cl (green) atoms cap the metal core along the C$_3$ axis with one p-ClPPh$_3$ ligand on the C$_3$ axis. In comparison with the **Au$_{11}$-H**, the **Au$_{11}$-Cl** crystal possesses a larger cell volume (23 297.7 Å^3 $versus$ 12 398 Å^3) and less density (2.066 g cm^{-3} $versus$ 2.243 g cm^{-3}), which is possibly attributed to distinct non-covalent interactions in the unit cell. More comparisons of the cell details are given in Table S1.†

The packing of these two nanoclusters along (100), (010), and (001) planes is shown in Fig. 3, respectively. For the T system of **Au$_{11}$-Cl**, the nanoclusters are organized layer by layer with an fcc-like ABCABC style viewing along a-axis, b-axis, and c-axis (Fig. 3a–c). Especially, viewing along the c-axis, the **Au$_{11}$-Cl** gets organized into a hexagonal lattice, while the **Au$_{11}$-H** gets decorated into a rectangular lattice. In the case of the **Au$_{11}$-H**, the nanoclusters are packed layer by layer with an ABAB style viewing along the a-axis, b-axis, and c-axis (Fig. 3d–f). Although the **Au$_{11}$-Cl** and the **Au$_{11}$-H** are constructed with the same core structure, they display totally different lattices. The obvious
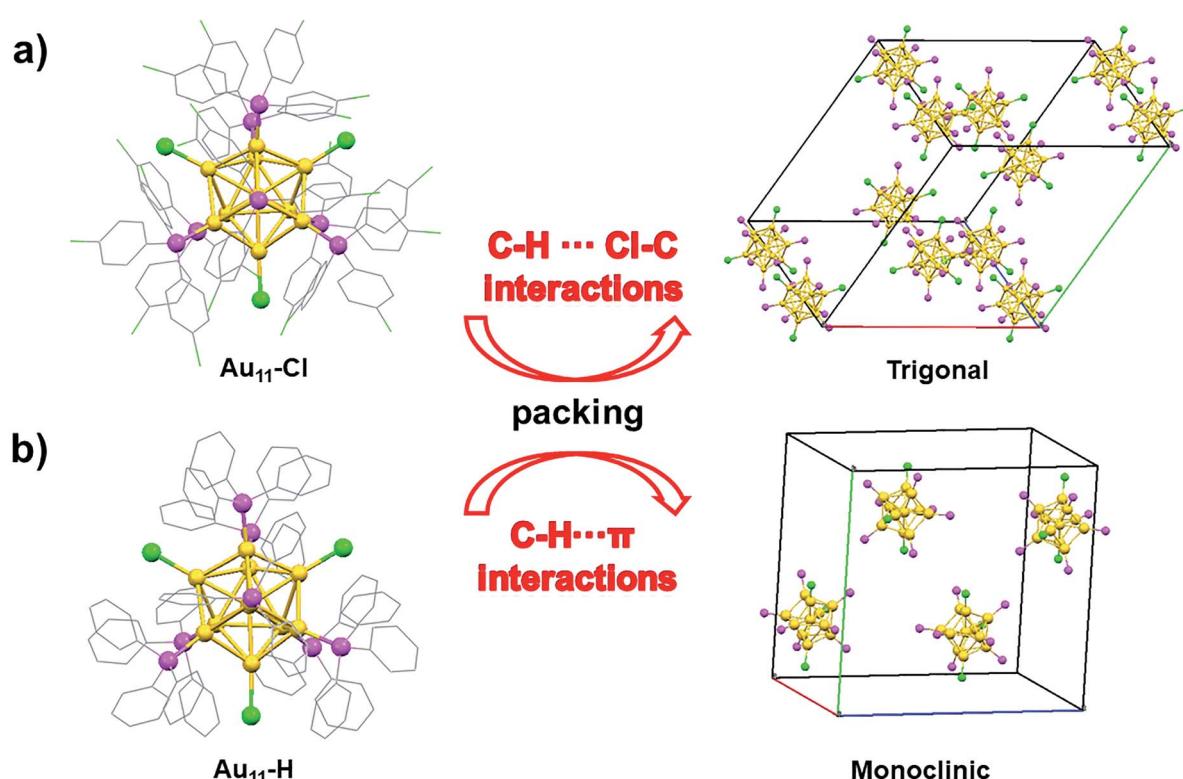

Fig. 2 (a) Crystal structure and trigonal unit cell of the **Au$_{11}$-Cl**. (b) Crystal structure and monoclinic unit of the **Au$_{11}$-H**. (colour labels: yellow = Au, pink = P, gray = C, green = Cl, for clarity all H atoms are not shown).
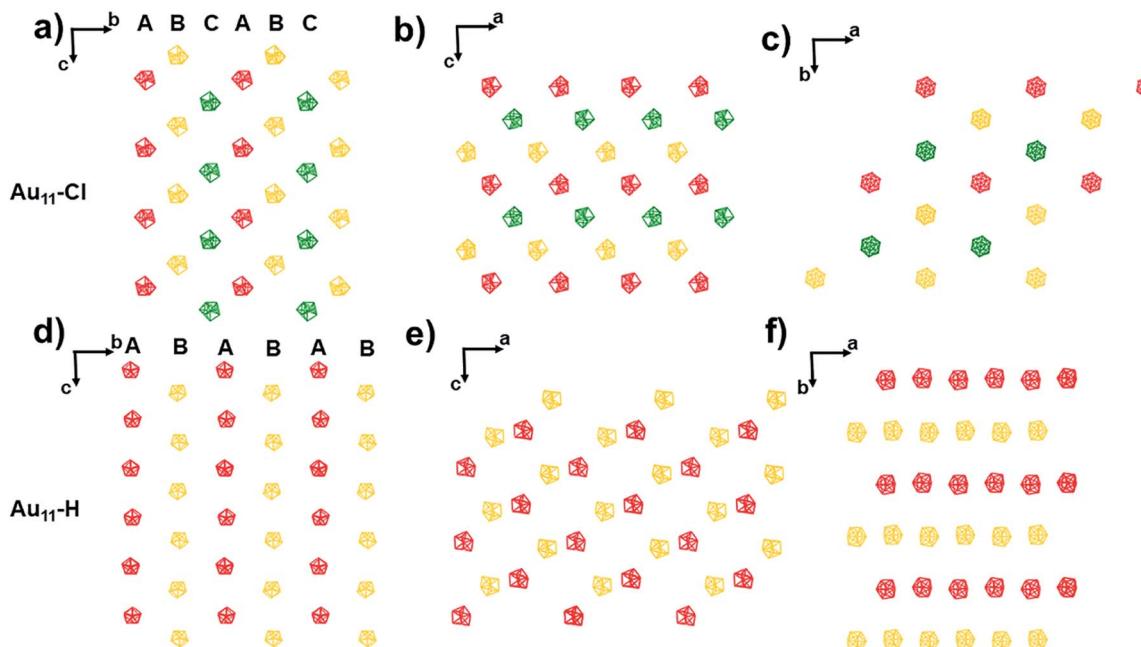
Fig. 3 Packing of the **Au$_{11}$-H** and the **Au$_{11}$-Cl** view from the (a and d) *a*-axis, (b and e) *b*-axis and (c and f) *c*-axis.

packing difference of the **Au$_{11}$** nanoclusters is related to the difference of non-covalent interactions between nanoclusters.[14]

C–H⋯π interactions play a crucial role in the crystal packing of the **Au$_{11}$-H**, which are the major driving force to form monoclinic. In the M system, each unit contains four **Au$_{11}$-H** nanoclusters. Fig. 4 shows the C–H⋯π interactions (red/blue dashed line) of the **Au$_{11}$-H**. C–H⋯π interactions exist between the C–H groups (blue) of the PPh$_3$ ligands and adjacent benzenes (green) of the adjacent cluster, evidenced by their distance. The distance of C–H⋯π ranges from 2.80 to 2.89 Å, with an average of 2.835 Å (Fig. S3†). Strong C–H⋯π interactions form a chain to hold each **Au$_{11}$-H** nanocluster and restrict the motion of the entire nanocluster.

Interestingly, most H atoms form C–H⋯π interactions are located on the *para* position of the benzene rings in the **Au$_{11}$-H**, which inspires us to speculate whether these interactions could be destroyed by introducing an atom with a larger atomic radius in the *para* position. As we expected, by replacing PPh$_3$ with *p*-ClPPh$_3$ ligands that contain Cl atoms on the *para* position of aromatic rings, C–H⋯π interactions are not found in the unit cell of the as-obtained **Au$_{11}$-Cl**. In order to discuss the non-covalent interactions of **Au$_{11}$-Cl**, four **Au$_{11}$-Cl** clusters are marked by the green quadrilateral (Fig. S7†).

As shown in Fig. 5, the inter-cluster distances are 19.80 Å and 17.42 Å, respectively, and the corresponding obtuse is 125.42°. However, the lengths (16.41 Å and 16.59 Å) and obtuse (127.86°) of **Au$_{11}$-H** are different from those of **Au$_{11}$-Cl**. When zooming into the surfaces between nanoclusters, C–H⋯Cl–C
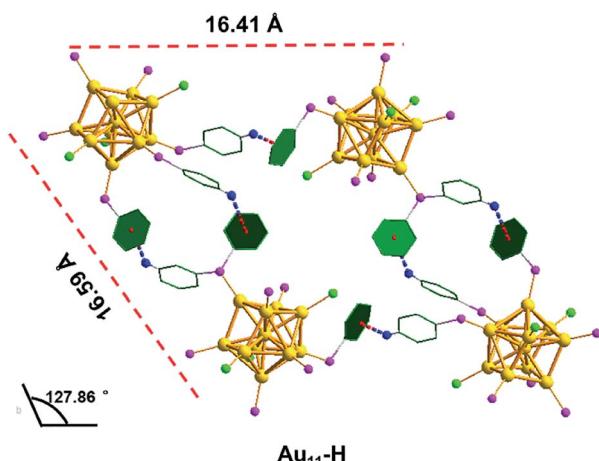
Fig. 4 The C–H⋯π interactions in the **Au$_{11}$-H**. Yellow = Au; pink = P; green = C; blue = H; bright green = Cl; blue red dashed, C–H⋯π interactions.
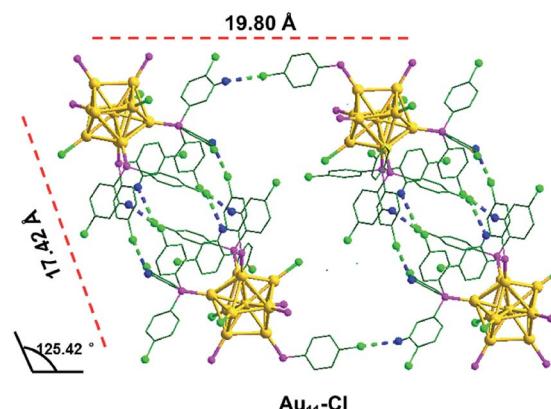
Fig. 5 The C–H⋯Cl–C interactions in the **Au$_{11}$-Cl**. Yellow = Au; pink = P; green = C; blue = H; bright green = Cl; bright green blue dashed, C–H⋯Cl–C interaction.
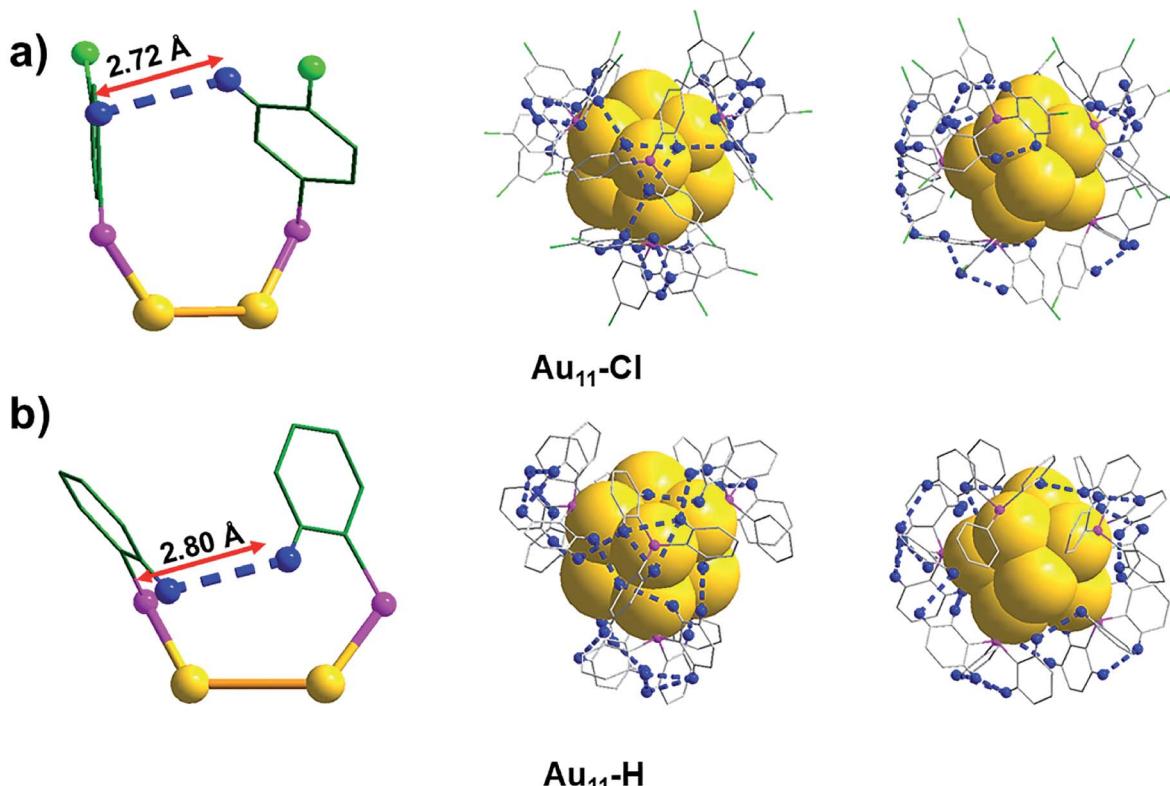
**Fig. 6** The nearest neighbour H and H atoms in the intra-**Au₁₁-Cl** and intra-**Au₁₁-H**. (a) The nearest neighbour H and H atoms in the **Au₁₁-Cl** viewed from different angles. (b) The nearest neighbour H and H atoms in the **Au₁₁-H** viewed from different angles. Yellow = Au; pink = P; green = C; blue = H; bright green = Cl; blue dashed, intra-D_{HH}; for clarity other atoms are not shown.

interactions (bright green/blue dashed line) of the **Au₁₁-Cl** lead to form T systems in the unit. In the T lattice of **Au₁₁-Cl**, the average distance of the C–H⋯Cl–C interactions is 2.94 Å, with a range from 2.85 to 2.99 Å (Fig. S4†). This distance is consistent with the reported value.[40] Overall, comparing the C–H⋯Cl–C interactions and the C–H⋯π interactions suggests that the insertion of chlorine atoms breaks C–H⋯π interactions and changes the crystal system from M to T.

Another significant aspect is that the non-covalent interactions of the intra-molecular also changed because of the introduction of chlorine atoms in the surface ligands. The average distance of H and H (D_{HH} for short) in the **Au₁₁-Cl** is 2.72 Å (Fig. 6a and S5†). In contrast, the D_{HH} in the **Au₁₁-H** is 2.80 Å, varying from 2.53 to 2.99 Å (Fig. 6b and S6†), which is slightly larger than that of the **Au₁₁-Cl**. Viewing along the C_3 axis, the

triangle constituted by nearest H atoms is slightly rotating compared with the one in **Au₁₁-Cl**, due to the introduction of the Cl atoms. The total numbers and average distances of the non-covalent interactions and the D_{HH} were shown in Table 1. All these results verify that non-covalent interactions of intra-cluster induce the rotation and arrangement of ligands, which further enable every single nanocluster to be compacted and ordered with reduced intra-cluster vibration, contributing to the formation of high-quality single crystals.

Conclusions

In summary, we have chosen the $Au_{11}(p\text{-ClPPh}_3)_7Cl_3$ (**Au₁₁-Cl**) and the $Au_{11}(PPh_3)_7Cl_3$ (**Au₁₁-H**) to investigate non-covalent interactions in the crystallization by surface modification. The chlorine atoms occupy the *para* of benzene rings in phosphine ligands, resulting in the breaking of C–H⋯π interactions and crystal system transformation. C–H⋯Cl–C interactions of $Au_{11}(p\text{-PPh}_3)_7Cl_3$ lead to the formation of trigonal systems, revealing the importance of the ligands on the non-covalent interaction modes. Moreover, UV-vis spectra and XPS spectra reveal the change of the electronic structure caused by surface modification. This work provides new insights into the effects of inter- and intra-interactions on nanocluster crystallization, making the assembly and self-assembly of metal nanoclusters more readily.

Table 1 The number of interactions for **Au₁₁-Cl** and **Au₁₁-H**

Interaction (distance)	**Au₁₁-H**	**Au₁₁-Cl**
CH⋯π	6 (2.84 Å)	×
C–H⋯Cl–C	×	20 (2.94 Å)
Inter-D_{HH}	46 (2.80 Å)	83 (2.81 Å)
Intra-D_{HH}	24 (2.79 Å)	21 (2.72 Å)

Conflicts of interest

There are no conflicts to declare.

Acknowledgements

Notes and references

1 R. Jin, C. Zeng, M. Zhou and Y. Chen, *Chem. Rev.*, 2016, **116**, 10346–10413.

2 I. Chakraborty and T. Pradeep, *Chem. Rev.*, 2017, **117**, 8208–8271.

3 J. Fang, B. Zhang, Q. Yao, Y. Yang, J. Xie and N. Yan, *Coord. Chem. Rev.*, 2016, **322**, 1–29.

4 H. Zhu, N. Goswami, Q. Yao, T. Chen, Y. Liu, Q. Xu, D. Chen, J. Lu and J. Xie, *J. Mater. Chem. A*, 2018, **6**, 1102–1108.

5 C. M. Aikens, *J. Phys. Chem. Lett.*, 2011, **2**, 99–104.

6 S. Xie, H. Tsunoyama, W. Kurashige, Y. Negishi and T. Tsukuda, *ACS Catal.*, 2012, **2**, 1519–1523.

7 M. Zhu, C. M. Aikens, F. J. Hollander, G. C. Schatz and R. Jin, *J. Am. Chem. Soc.*, 2008, **130**, 5883–5885.

8 P. D. Jadzinsky, G. Calero, C. J. Ackerson, D. A. Bushnell and R. D. Kornberg, *Science*, 2007, **318**, 430–433.

9 Y. Wang, X. K. Wan, L. Ren, H. Su, G. Li, S. Malola, S. Lin, Z. Tang, H. Hakkinen, B. K. Teo, Q. M. Wang and N. Zheng, *J. Am. Chem. Soc.*, 2016, **138**, 3278–3281.

10 C. P. Joshi, M. S. Bootharaju, M. J. Alhilaly and O. M. Bakr, *J. Am. Chem. Soc.*, 2015, **137**, 11578–11581.

11 Z. Wu, Q. Yao, S. Zang and J. Xie, *ACS Mater. Lett.*, 2019, **1**, 237–248.

12 M. Zhu, S. Jin and S. Wang, *Chem.–Asian J.*, 2019, **14**, 3222–3231.

13 R. W. Huang, Y. S. Wei, X. Y. Dong, X. H. Wu, C. X. Du, S. Q. Zang and T. C. W. Mak, *Nat. Chem.*, 2017, **9**, 689–697.

14 N. Yan, N. Xia, L. Liao, M. Zhu, F. Jin, R. Jin and Z. Wu, *Sci. Adv.*, 2018, **4**, eaat7259.

15 X. Kang, Y. Song, H. Deng, J. Zhang, B. Liu, C. Pan and M. Zhu, *RSC Adv.*, 2015, **5**, 66879–66885.

16 A. Nag, P. Chakraborty, M. Bodiuzzaman, T. Ahuja, S. Antharjanam and T. Pradeep, *Nanoscale*, 2018, **10**, 9851–9855.

17 S. Kumar and R. Jin, *Nanoscale*, 2012, **4**, 4222–4227.

18 P. Chakraborty, A. Nag, A. Chakraborty and T. Pradeep, *Acc. Chem. Res.*, 2019, **52**, 2–11.

19 P. Sun, Z. Wang, Y. Bi, D. Sun, T. Zhao, F. Zhao, W. Wang and X. Xin, *ACS Appl. Nano Mater.*, 2020, **3**, 2038–2046.

20 Z. Wu, J. Liu, Y. Gao, H. Liu, T. Li, H. Zou, Z. Wang, K. Zhang, Y. Wang, H. Zhang and B. Yang, *J. Am. Chem. Soc.*, 2015, **137**, 12906–12913.

21 Z. Wu, C. Dong, Y. Li, H. Hao, H. Zhang, Z. Lu and B. Yang, *Angew. Chem., Int. Ed.*, 2013, **52**, 9952–9955.

22 J. Fontana, W. J. Dressick, J. Phelps, J. E. Johnson, R. W. Rendell, T. Sampson, B. R. Ratna and C. M. Soto, *Small*, 2014, **10**, 3058–3063.

23 M. De Nardi, S. Antonello, D.-e. Jiang, F. Pan, K. Rissanen, M. Ruzzi, A. Venzo, A. Zoleo and F. Maran, *ACS Nano*, 2014, **8**, 8505–8512.

24 P. Chakraborty, A. Nag, G. Paramasivam, G. Natarajan and T. Pradeep, *ACS Nano*, 2018, **12**, 2415–2425.

25 V. Berry and R. F. Saraf, *Angew. Chem., Int. Ed.*, 2005, **44**, 6668–6673.

26 K. Müller-Dethlefs and P. Hobza, *Chem. Rev.*, 2000, **100**, 143–168.

27 Y. Song, S. Weng, H. Li, H. Yu and M. Zhu, *Inorg. Chem.*, 2019, **58**, 7136–7140.

28 S. Zhang, X. Lu, J. Sun, Y. Zhao and X. Shao, *CrystEngComm*, 2015, **17**, 4110–4116.

29 X. Kang and M. Zhu, *Coord. Chem. Rev.*, 2019, **394**, 1–38.

30 Z. Gan, J. Chen, J. Wang, C. Wang, M.-B. Li, C. Yao, S. Zhuang, A. Xu, L. Li and Z. Wu, *Nat. Commun.*, 2017, **8**, 14739.

31 M. R. Narouz, S. Takano, P. A. Lummis, T. I. Levchenko, A. Nazemi, S. Kaappa, S. Malola, G. Yousefalizadeh, L. A. Calhoun, K. G. Stamplecoskie, H. Hakkinen, T. Tsukuda and C. M. Crudden, *J. Am. Chem. Soc.*, 2019, **141**, 14997–15002.

32 H. Yang, Y. Wang, H. Huang, L. Gell, L. Lehtovaara, S. Malola, H. Hakkinen and N. Zheng, *Nat. Commun.*, 2013, **4**, 2422.

33 Q. Yao, Y. Yu, X. Yuan, Y. Yu, D. Zhao, J. Xie and J. Y. Lee, *Angew. Chem., Int. Ed.*, 2015, **54**, 184–189.

34 J. Liang, X.-S. Wu, X.-L. Wang, C. Qin, K.-Z. Shao, Z.-M. Su and R. Cao, *CrystEngComm*, 2016, **18**, 2327–2336.

35 J. Shen, Z. Wang, D. Sun, G. Liu, S. Yuan, M. Kurmoo and X. Xin, *Nanoscale*, 2017, **9**, 19191–19200.

36 L. C. McKenzie, T. O. Zaikova and J. E. Hutchison, *J. Am. Chem. Soc.*, 2014, **136**, 13426–13435.

37 Z. Qin, D. Zhao, L. Zhao, Q. Xiao, T. Wu, J. Zhang, C. Wan and G. Li, *Nanoscale Adv.*, 2019, **1**, 2529–2536.

38 Y. Shichibu, Y. Negishi, T. Tsukuda and T. Teranishi, *J. Am. Chem. Soc.*, 2005, **127**, 13464–13465.

39 M. R. Narouz, K. M. Osten, P. J. Unsworth, R. W. Y. Man, K. Salorinne, S. Takano, R. Tomihara, S. Kaappa, S. Malola, C. T. Dinh, J. D. Padmos, K. Ayoo, P. J. Garrett, M. Nambo, J. H. Horton, E. H. Sargent, H. Hakkinen, T. Tsukuda and C. M. Crudden, *Nat. Chem.*, 2019, **11**, 419–425.

40 P. K. Thallapally and A. Nangia, *CrystEngComm*, 2001, **3**, 114–119.